ORIGINAL ARTICLE

New drawbead tester and numerical analysis of drawbead closure force

Imanol Gil[1] · Joseba Mendiguren[1] · Lander Galdos[1] · Endika Mugarra[1] · Eneko Saenz de Argandoña[1]

Abstract

Currently, a great deal of controversy exists regarding the real forces generated in drawbeads during sheet metal forming processes. The present work focuses on the analysis of the uplift force. First, a detailed literature review is carried out to analyse previous experimental procedures used to measure uplift forces. It is found that previous setups do not perfectly replicate the real geometry of industrial drawbeads. In order to obtain reliable forces, an experimental drawbead tester capable of adequately replicating industrial drawbeads is developed. Later, a variety of steels ranging from mild steels to 3rd-generation ultra-high-strength steels are tested and reliable uplift and also restraining force values are obtained. The main purpose of the work is to share with the research community reliable experimental data that allows precise evaluation of the accuracy of current drawbead models and that supports the generation of new numerical and equivalent drawbead models. In parallel to the experimental procedure, a step forward in the understanding of the drawbead closing phenomena is also achieved through a 2D numerical model. The main purpose of the model is to identify the variables that greatly affect uplift force. Going beyond previous studies, in which some variables were analysed, the present work covers, in a holistic manner, the impact that material properties, the geometry of drawbeads and contact behaviour between sheet and drawbead have on the uplift force. It is determined that surprisingly minor geometrical deviations in the drawbead nominal geometry have a large impact on the uplift force.

Keywords Drawbead tester · Uplift force · Restraining force · Numerical modelling · Geometrical deviations

1 Introduction

The use of drawbeads is an extensive practice within the automotive die manufacturing industry. Alves et al. [1] already pointed out that drawbeads are an essential element in developing a successful deep drawing process for a large number of automotive components, due to the fact that they are the elements within the stamping tool that, in combination with the frictional work, define the restraining level to the flow of the sheet in the blankholder area. By modifying the dimensions of the drawbead, the level of restraining can be controlled by the die designers. Through numerical simulations, an iterative optimization process is carried out in which, among other process parameters, the dimensions of the drawbeads are

modified to ensure the required strain and stress distribution among the components.

The physical implementation of drawbead geometry in the deep drawing simulation increases the computational time due to the reduced drawbead dimensions in comparison to the component that is formed. Therefore, over the course of the industry's history, numerous analytical drawbead models, also called equivalent drawbead models, have been developed. As described by Courvoisier et al. [2], the main purpose of equivalent drawbead models is to predict the forces produced in drawbeads, thereby avoiding their physical implementation, in numerical simulations. In this manner, the physical drawbead can be substituted with a line where an uplift force, a restraining force and a strain are applied to the elements that cross that line.

Developing an understanding of the restraining force applied to the sheet in the drawbead is the main objective when applying drawbeads in drawing operations. In this context, Li et al. [3] have already pointed out that most of the previous research has focused on analysing the restraining phenomena of the sheet. The very first experimental analysis of drawbead

✉ Imanol Gil
  esaenzdeargan@mondragon.edu

1 Mechanics and Industrial Production Department, Mondragon Unibertsitatea, Loramendi 4, Mondragon, 20500 Gipuzkoa, Spain

forces was conducted by Nine in 1978 [4]. Nine's research focused on analysing the friction found in circular geometries and developed a tool constructed with rolls that attempted to replicate the geometry of a drawbead. In his experiments, Nine forced the sheet to go through the rolls, thereby blocking their rotation in some experiments and allowing them to rotate in other experiments. He considered that the differences observed in the restraining force were generated by the friction and calculated the coefficient of friction observed in the cylindrical surfaces of the rolls. Even if the geometry of the tooling used by Nine did not perfectly replicate the geometry of a drawbead, the experimental results obtained were adopted as a reference and used to validate the initial equivalent drawbead models developed later. In fact, Nine [5] developed an experimental database for several materials, thicknesses and tool geometries that he expanded through analysis of more materials and thicknesses in 1982.

Following these initial works, and due to the importance of an accurate prediction of the restraining force (as mentioned previously), the research community has traditionally paid more attention to analyse the restraining force. Therefore, many more studies focused on restraining force can be found than studies focused on uplift force. At this point, it must be considered that correctly predicting the uplift force is extremely important as well. The force exerted by the binder is divided into the force necessary to close the drawbeads (the uplift force) and the force that generates the contact pressure on the sheet. If the force required to close the drawbeads is not correctly predicted and an error is also made in the prediction of the contact pressure distributed along the sheet in the blankholder area, as already identified by Bolay et al. [6], the frictional restraining force between the sheet and the tools will not be correctly predicted, resulting in substantial differences between numerical and experimental results.

These differences have an impact on the formability and final geometric prediction of the components. Gil et al. [7] already proved this by showing that numerical errors in the predicted frictional forces generate substantial differences in the final numerical predicted geometry when compared to the experimental one. Furthermore, Leocata et al. [8] have recently proved the importance of the binder pressure zones in the robustness of the restraining force, demonstrating that the contact pressure achieved in the inner ring of the drawbead is of high importance and determines the stability of the drawing process. Therefore, an accurate prediction of the uplift force is also important for the optimum performance of drawing tools. Finally, and as a clarification, it must also be stated that although a large percentage of stamping companies use spacers to control the parallelism and to tune the restraining force, it is mandatory for toolmaker companies to ensure the correct performance of the tool set without the use of spacers. For this reason, the correct prediction of the uplift force (and therefore the binder force) is of critical importance for correct die design

and die performance (including the press-line capability analysis).

Taking all of this into consideration, a review of the research works focused on the development of analytical models for the prediction of the uplift force is undertaken. In 1986, Triantafyllidis et al. [9] developed an analytical model to identify the strains and stresses imposed on the material when going through the drawbead. Although the purpose of the model was to identify potential areas in which the material could be broken, the uplift and restraining forces were also predicted. During their investigations, Triantafyllidis et al. found that contrary to the effect on the restraining force, friction has a negligible effect on the uplift force. As a continuation of the work of Triantafyllidis et al., Maker et al. [10] conducted an experiment designed to measure both uplift and restraining forces. When comparing restraining forces, Maker et al. found a positive agreement with the analytical results for certain conditions although differences of up to 18% were found for others. In terms of uplift force, the experimental uplift force was measured at a distance to perfect closure of 10% of the sheet thickness. Therefore, this should not be considered to be the genuine uplift force. Furthermore, differences between the experimental and analytically predicted forces of up to 50% were found.

In 1988, Stoughton [11] developed the most widely used drawbead equivalent model. The basis of the model is that the restraining force is equal to the force necessary to bend and unbend the material in addition to the friction that the sheet must overcome when going through the drawbead. The shape of the sheet when going through the drawbead was considered symmetric and the geometry of the sheet was assumed to be tangent to the different radius of the drawbead. Therefore, the restraining force was based on the material properties, the coefficient of friction, the sheet thickness and the geometry of the drawbead. The uplift force was calculated by considering the vertical reaction of the forces previously calculated for the prediction of the restraining force. Stoughton validated his model by comparing his results with the experimental results obtained by Nine in 1982 [5], finding a positive agreement in the case of the restraining forces. In the case of the uplift forces, the differences were in the range of 10%. At this point, however, it must be remembered that the setup of Nine's experiments does not accurately represent the geometry of real drawbeads, as previously mentioned.

L. R. Sanchez et al. [12] developed in 1996 an equivalent drawbead model in which the non-symmetrical shape of the sheet when going through the drawbead was also considered. Based on the incremental plasticity approach already used by Wang [13], prediction of the strain evolution of the material through its thickness was accomplished. Thereby, the internal stresses at each point of the material, as well as the reactions exerted by the sheet to the drawbead, were calculated. The analytical results were compared with the ones obtained by

Nine in 1978 and differences of up to 9% were found in the case of the restraining force and 15% in the case of the uplift force. The researchers argued that these differences were due to the non-modelization of the strain rate of the material. Another important aspect of the work is its description of the lack of a standardized test for the measurement of the restraining and uplift forces, which impacts the experimental results in terms of causing high variability.

Y.T. Keum et al. [14], based on the model previously developed by Stoughton [11], developed an analytical model capable of combining different drawbead geometries. The basic concept of the model is that when two drawbeads are placed one after the other, the restraining and uplift forces of each individual drawbead can be considered a sum. For example, they described the combination of a step and a circular drawbead, adding the forces exerted by the surfaces, which are in the lateral area of the drawbead punch, arguing that those surfaces were also generating reaction forces that must be considered. This had not been previously taken into account and as will be proved later is of great importance for the prediction of uplift forces. Y.T. Keum et al. compared the restraining results of his model with experimental results obtained by Kim and Choi [15]. They found a positive agreement in terms of restraining force and material strains, although no comparison with experimental data was made in the case of the uplift forces.

Yang et al. [16] also developed a 2D numerical model for the prediction of uplift forces carrying out an experimental measurement of uplift forces in parallel. When comparing the results, they found very similar results for the numerical and experimental results. It must be stated, however, that as in the work of Kim et al. [17] they used spacers that prevented a complete closure of the drawbead.

Firat [18], as Y.T. Keum et al. previously did, modified the model proposed by Stoughton [11] with the purpose of considering the flow direction of the material with respect to its rolling direction. He compared the results with the experimental results obtained by Green [19]. It must be noted that Green used spacers in his experimental setup, which avoided the complete closure of the drawbead. The gap left between the sheet and the tools was 0.4mm. When comparing the results, Firat found a difference of up to 38% in the case of the restraining force for high-strength steels. No comparison was made for uplift forces.

Moon et al. [20] modified the drawbead model developed by Y.T. Keum et al. [14] including an anisotropic yielding criterion developed by Barlat [21] and the kinematic hardening model developed by Chaboche [22]. They analysed different drawbead geometries and compared the results of the analytical model with numerical results obtained in the same research work through a 2D numerical model. They found differences of up to 5% in the case of the restraining forces

and up to 17% in the case of the uplift force. No comparison was made with experimental results.

The previous studies focused on predicting the uplift and restraining forces and used analytical and/or numerical models to do so. However, and as pointed out by Xu et al. [23], numerical modelization is also a powerful tool for understanding the material behaviour within the drawbead. Following this idea, some works are found in which numerical modelization is used to better understand the interaction of the material with the drawbead. Choi et al. [24] used a numerical model to analyse the evolution of the uplift force during the drawbead closure. They found 40% of the uplift force to be generated during the last 0.5 mm of the closure. Kim et al. [17] also developed a numerical model and found the same uplift force trend during the drawbead closure. Furthermore, they also carried out experimental tests in order to compare the numerical and experimental results. Even if they left a 0.1-mm gap in the experimental tests, they observed the same uplift force trend with a large increment in the last tenths of millimetres. When they compared the numerical results and the experimental results, they found the predicted numerical results to be much higher than the experimental results actually measured.

A very interesting analysis using numerical methods was carried out by Larsson et al. [25]. Larsson developed a numerical model using shell elements for a round drawbead. The particularity of this numerical model is that Larsson divided the upper portion of the drawbead into two sub-bodies. The first sub-body encompassed the drawbead punch, and the second sub-body was composed of the horizontal surfaces on the lateral side of the punch. Larsson discovered in the numerical results that the uplift force was mainly governed by these lateral surfaces, which generated up to 90% of the total uplift force.

Larsson's conclusion, together with the uplift force evolution observed in both the numerical and experimental results described above, indicates that previous experimental setups failed to represent the real conditions of industrial drawbeads. Nine setups in his experimental tests in 1978 and 1982 used cylindrical rolls rather than flat surfaces. A perfect closure of the drawbead was thus not achieved. Later and as described previously, Yellup and Painter [26], Maker et al. [10], Kim et al. [17], Yang et al. [16], Green [19] and Firat [18] also carried out uplift force experimental measurements, but in all of the cases, a gap between the sheet and the horizontal surfaces on the lateral side of the punch was left. The assertion can therefore be made that no experimental results can be found in the literature that measure uplift forces fairly.

Hence, the main objective of this work is to develop a reliable and realistic drawbead tester in order to be able to accurately measure uplift as well as restraining forces in drawbeads. For this purpose, an experimental drawbead tester capable of adequately reproducing the existing forces in an

industrial drawbead is developed. Next, a variety of steels of different resistances are tested in order to obtain the uplift and restraining forces produced by several bead heights. Mechanical and tribological properties of the steels are also characterized and clearly presented in the paper. All of these results will serve as a database with which to correctly evaluate the accuracy of actual and future drawbead numerical and equivalent models. In parallel with the experimental procedure, a better understanding of drawbead closing phenomena is also achieved by means of a 2D numerical model. The main purpose of this model is to identify variables with the greatest effect on uplift force. Beyond previous research that analyses only certain variables, the present work holistically examines the impact of material properties, the contact behaviour between the sheet and the drawbead and the geometry of the drawbead on the uplift force. Surprisingly minor geometrical deviations in the drawbead nominal geometry are found to have a large impact on the uplift force. This finding has never been reported previously and may be the reason for the large discrepancies between the predictions of current analytical models and the real uplift forces observed in the industry.

2 Materials and methodology

2.1 Mechanical characterization

To determine the mechanical properties of the steels investigated in this study, uniaxial tensile tests were conducted in accordance with ASTM E8-04 standards with a constant strain rate of $6 \times 10^{-4} \, s^{-1}$. The selected materials cover a wide range of the steels used in deep drawing automotive components from a mild steel of approximately 150 MPa of yield strength up to an ultra-highstrength steel of approximately 700 MPa of yield strength. The experimentally obtained stress-strain curves of the investigated steels are depicted in Fig. 1.

Moreover, Lankford coefficients were calculated from standard tensile tests at 0, 45 and 90° to the rolling direction
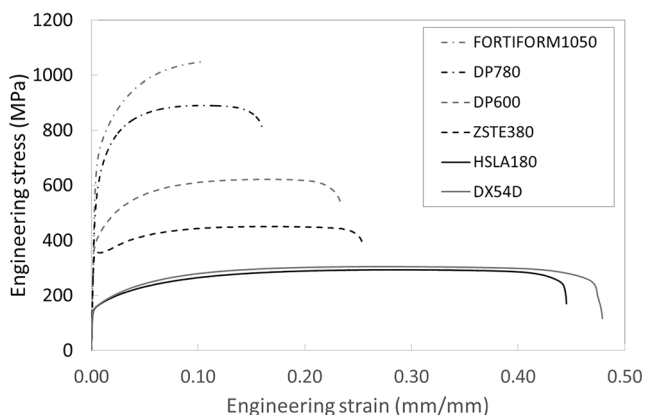

Fig. 1 Tensile test curves in rolling direction of the six steels studied

using GOM Aramis DIC system. Table 1 depicts the main mechanical properties achieved in the tensile tests.

2.2 Tribological characterization

Triantafyllidis et al. [27] already pointed out that the definition of the contact between the sheet and the drawbead tools is a key factor in correctly predicting drawbead forces. Lee et al. [28] observed a 15% increase in the restraining force due to an increase of 0.05 in the value of the coefficient of friction. Moreover, Sriram et al. [29] observed the contact pressure distribution in a round drawbead to lie within a range of 1 to 15 MPa, aside from very localized contact points, at which 500 MPa of contact pressures was observed.

In light of statements affirming that the contact pressure influences the coefficient of friction [7], strip drawing tests were conducted at different contact pressures. In order to represent industrial die surface conditions, the tools in contact with the sheets were machined and polished thereafter in accordance with die manufacturer standards. A hardened 1.2379 steel commonly used to make die tools was utilized to fabricate the tools. The tool properties are summarized in Table 2.

Figure 2 presents the coefficient of friction measured for each of the steels at different contact pressures.

A similar behaviour can be observed for all of the materials studied. Each of the materials demonstrates a decrement tendency for the coefficient of friction value as the contact pressure increases. This decrement of the coefficient of friction is the result of the flattening of the asperities that the sheet surface suffers when the contact pressure is increased moving the tribo-system from a boundary lubrication state to a mixed lubrication state. This finding aligns with previous results, such as those provided by Sigvant et al. [30].

2.3 Characterization of drawbead forces

An experimental setup that fairly reproduces the geometry of industrial round drawbeads was manufactured. Figure 3 schematically presents the geometry of the drawbead. The main geometrical variables that define the drawbead are the punch radius, the punch height, the female width and the entrance and exit radius of the female.

The punch radius and entrance and exit radius of the female were kept constant for all of the experiments. The values selected for these variables, based on industry standards, are 5 mm for the punch radius and 3 mm for both the entrance and exit radius of the female. In the case of the female width, again in line with industry standards, the value was modified according to the thickness of the material to be tested. Thus, the female width (w) is calculated as w= 2 *R + 3* t, where R is the value of the punch radius and t refers to the thickness of the material (see Table 1). Finally, the height of the punch was increased from 2 to 5mm. Table 3 presents the test conditions

Table 1 Summary of the main mechanical properties obtained from the standard tensile tests

Material	DX54D	HSLA180	ZstE380	DP600	DP780	FF1050
Thickness (mm)	0.60	0.64	1.35	1.51	1.49	1.57
Young modulus E (GPa)	206	200	208	197	198	194
Yield strength (MPa)	151	151	353	393	540	687
UTS (MPa)	308	304	452	622	893	1047
Elongation at Rm A_{Rm} (%)	23	25	16	16	10	10
r0 (-)	1.9	2.0	0.7	0.8	0.7	0.8
r45 (-)	1.8	1.7	1.1	0.9	0.9	0.9
r90 (-)	1.6	2.4	0.9	1.1	0.9	1.0

for each material (refer to Fig. 3 for a description of the dimensions). Specimens 30 mm in width and 400 mm in length were precut. Before conducting the test, the edges were manually polished in order to avoid edge cracks that could interrupt the experiments and/or degrade the tools.

The drawbead is composed of two parts, a lower part containing the female and an upper part comprised of the punch and the horizontal lateral surfaces. Both the upper part and the lower part were designed in a modular way with the aim of using inserts to modify the different dimensions of the drawbead in accordance with Table 3. In the upper part, the height of the drawbead punch can be modified with the introduction of calibrated blocks. In the lower part, the groove width can also be varied with the implementation of inserts.

The lower part of the tool remains static and is attached to the bench of a 100-kN Instron compression machine. The upper part, which is mobile, is attached to the crossbar of the compression machine. Both parts of the tooling are guided together by four columns and special ball guiding systems. The use of ball guiding ensures an accurate relative positioning of the female and punch as well as the absorption of lateral forces that could introduce noise in the measurement of the vertical force. The compression machine is used as the actuator to perform the vertical displacement and to close the drawbead punch in the female. A linear SKF electric actuator is responsible for pulling the material through the drawbead. The measurement of the uplift force is carried out by means of the compression machine 100-kN load sensor. For the restraining force, a 10-kN load sensor was introduced in the axis of the linear electric actuator. Figure 4 depicts a 3D representation of the drawbead tooling developed.

A two-step characterization procedure was carried out. Initially, closing tests were conducted to measure the uplift

Table 2 Surface properties of the tools used in the strip drawing test

Material	R_a (μm)	Surface finishing	Hardness (HRc)
1.2379	0.4	Manual polishing	60

force. These tests were performed by commanding the compression machine crossbar at a predefined velocity of 100mm/min in the drawbead closing direction. In the closing step, the displacement was recorded by a LVDT sensor attached to the upper plate of the tool where the punch is attached. Simultaneously, the signal of the compression machine load cell was obtained. As the drawbead closed, the force recorded in the compression machine's load sensor increased progressively until reaching a point at which a sudden force increment took place (see Fig. 6). The sudden force increment was produced as a result of the impact that takes place when the drawbead completely closes. To better identify the change in the force slope that represents the exact value of the uplift force, kissing-blocks were added at the laterals of the specimen so as to provide a higher rigidity at the closing point. The kissing-blocks, pre-cut squares of the same material in order to guarantee the same thickness as the specimen, significantly increased the change in the force slope at the drawbead perfect closure. Their implementation thus facilitated identification of the instant at which the complete drawbead closure occurred. Figure 5 shows the area where the kissing-blocks are placed more clearly.

Figure 6 depicts an uplift force curve obtained in a closing test. It can be observed that the force initially increased slowly. However, as the closure point was approached, the force slope increases, especially during the last twenty hundredths of 1 mm. When reaching the closure point, the force curve suddenly changes to a vertical slope, which indicates that the relative distance between the drawbead punch and the female no longer changes. In fact, due to the impact, even a slight backward motion can be observed, as the upper plate underwent a small degree of tilt.

Once the uplift force was identified, the restraining force was also measured. Restraining tests were carried out for this purpose with the same experimental setup. The restraining tests were divided into the 3 phases as shown in Fig. 7.

1. Phase 1: First, the drawbead was closed. In this phase, the compression machine was commanded to reach the uplift force measured in the closing tests.
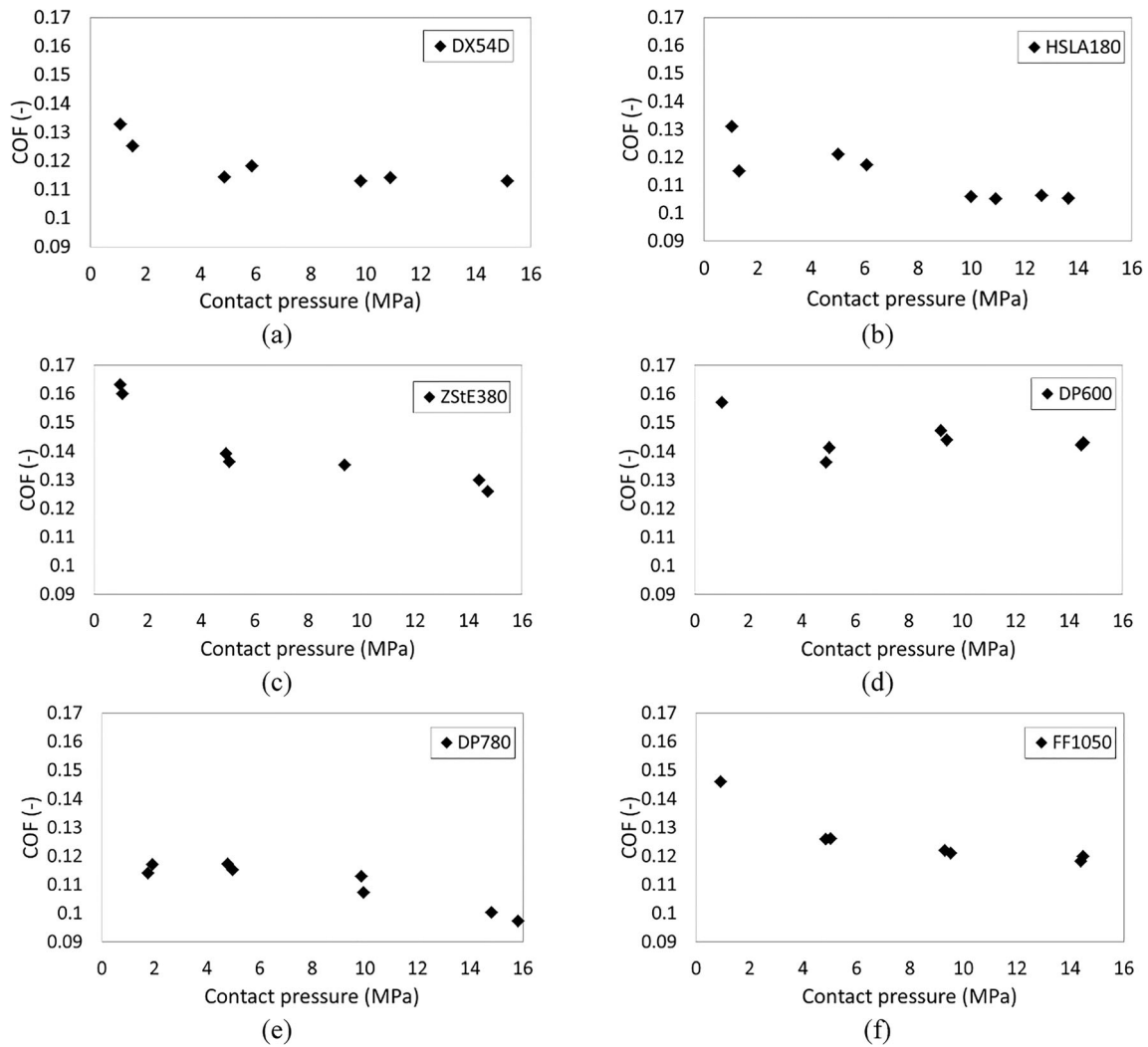
Fig. 2 Strip drawing test results at different contact pressures for (a) DX54D, (b) HSLA180, (c) ZStE380, (d) DP600, (e) DP780 and (f) Fortiform1050

2. Phase 2: After the force stabilization, which took several seconds, an opening of five hundredths of 1 mm was induced. This procedure ensured that when the specimen was pulled out of the drawbead, the horizontal surfaces at the lateral of the drawbead did not block the specimen.

3. Phase 3: Finally, the linear actuator pulled the specimen out of the drawbead at a predefined velocity of 10 mm/s.

The compression machine crossbar was commanded to maintain the position previously reached. During this phase, both force signals were recorded. The signal obtained from the horizontal axis corresponds to the restraining force. The signal obtained from the vertical axis, i.e. from the compression machine load cell, corresponds to the uplift force necessary to keep the drawbead
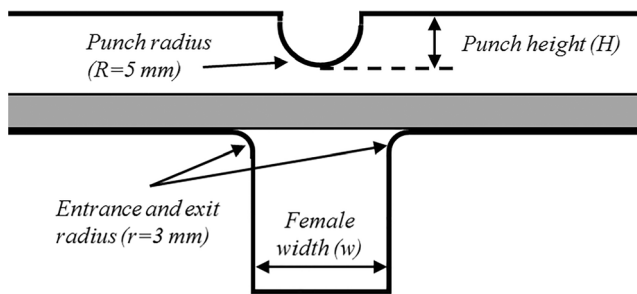
Fig. 3 Graphic representation of the main dimensions of the drawbeads tested

Table 3 Drawbead dimensions for each of the materials tested

Material	Punch height, H (mm)	Groove width, w (mm)
DX54D	2-3-4-5	11.8
HSLA180	4-5	11.8
ZStE380	2-3-4	14.5
DP600	2-3-4	14.5
DP780	2-3-4-5	14.5
Fortiform1050	2-3-4	14.5
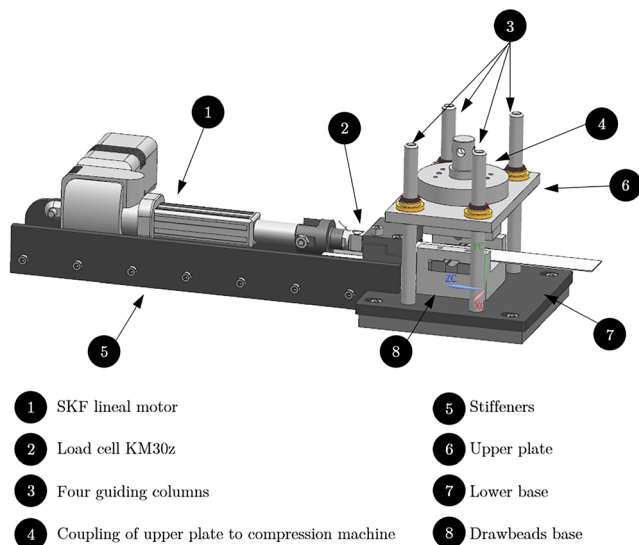
Fig. 4 Depiction of the drawbead tooling

|	
1 SKF lineal motor	5 Stiffeners
2 Load cell KM30z	6 Upper plate
3 Four guiding columns	7 Lower base
4 Coupling of upper plate to compression machine	8 Drawbeads base

closed during the sheet flow. It must be noted that, depending on the drawbead geometry, the initial uplift force necessary to close the drawbead and the uplift force necessary to maintain this position during the sheet flow may not be the same. The present work focuses on the first force, the so-called uplift force for drawbead complete closure, as presented in Fig. 8.

Figure 8 shows both forces during a restraining test. In the case of the uplift force, the value initially achieved is the uplift force predefined by the user that was calculated in the closing tests. Next, the uplift force decreased when the machine moved up five hundredths of 1 mm. Finally, the uplift force during the sheet flow was recorded, as was the restraining force. It can be observed that no restraining force was measured until the specimen was pulled through the drawbead.
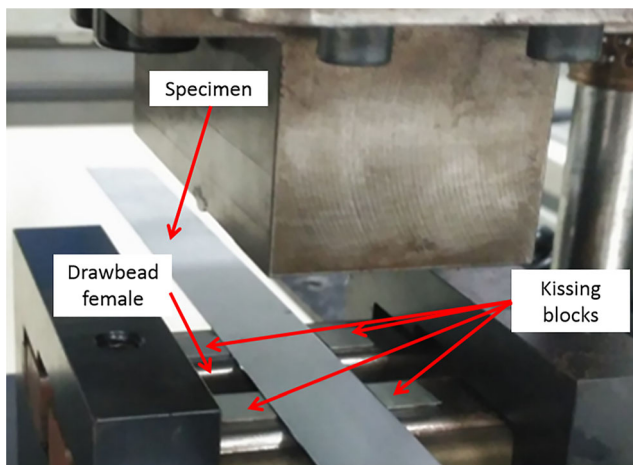
Fig. 5 Setup of the kissing-blocks on the drawbead test tool to measure the uplift force
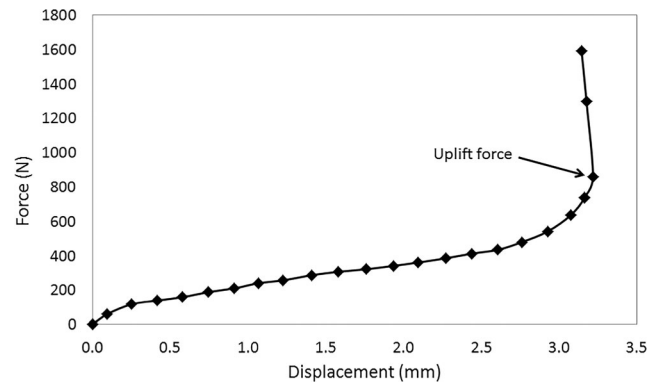
Fig. 6 Evolution of the uplift force as tools close. The arrow indicates the moment of complete closure, in which the force increases sharply

Note again that the analysis carried out in the present study focuses on the initial uplift force generated to close the drawbead.

3 Numerical modelling

3.1 Numerical model definition

As mentioned in Section 1, many researchers focused their efforts on developing a better understanding of the material's behaviour while flowing through the drawbead. However, previous research generally did not analyse the closing phase of the drawbead. The present research thus focused on gaining insight into the phenomena taking place during the drawbead closing phase.

With this aim, a 2D numerical model was developed. For this purpose, the geometry of the drawbead was modelled as depicted in Fig. 9. The tool is composed of two main rigid bodies, a lower body representing the drawbead female and an upper body representing the drawbead punch and the lateral flat surfaces. This upper body was sub-divided into two sub-bodies: the punch and the flat surfaces on the lateral side of the punch. The main reason for this sub-division was to enable the analysis of the contribution of the punch and the lateral surfaces to the uplift force. Both the lower body and the two upper bodies were modelled as solid rigid surfaces. The last component of the 2D numerical model was the sheet, which was defined as a deformable body. The sheet was comprised of a mesh of quadrilateral "plane strain" elements of 4 nodes and reduced integration designated as CPE4R in Abaqus. Eleven elements were defined in the thickness direction (therefore 11 integration points through thickness), a number adequate for obtaining accurate results [31]. The sheet was therefore composed of 11 elements in the thickness direction, with each element having a height of 0.135 mm. A total of 14,762 elements make up the sheet.

Concerning the boundary conditions, the lower body, drawbead female, was fixed, while the upper body, punch
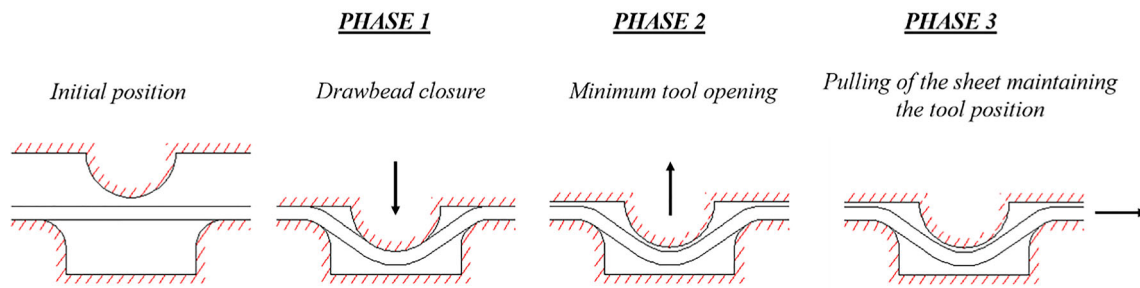
Fig. 7 Graphic presentation of the different stages of the drawbead restraining test

together with the lateral surfaces, moved down until reaching the complete closure. The complete closure was reached when the distance between the horizontal surfaces lateral to the punch and the horizontal surfaces of the drawbead female was equal to the thickness of the sheet. As in the experimental tests, the entrance and exit radius of the drawbead female had a value of 3 mm, while the punch radius had a value of 5 mm.

In order to use a representative case for this numerical analysis, a 3-mm punch height was defined, and a DP780 high-strength steel was implemented as the sheet material. The hardening of the material was defined by the Combined Swift-Hockett Sherby model [32]. The parameters that fit the behaviour of the material measured in the previously mentioned tensile tests are presented in Table 4. An anisotropic Hill48 yield criterion was used.

In terms of tribological conditions, based on the results obtained in the tribological characterization, a pressure-dependent coefficient of friction was defined. The results obtained from the strip drawing test at different contact pressures for DP780 were utilized for this purpose (see Fig. 2).

3.2 Numerical sensitivity analysis

A sensitivity analysis that took advantage of the previously mentioned numerical model was conducted in order to better evaluate the model parameters' influence on the uplift force.
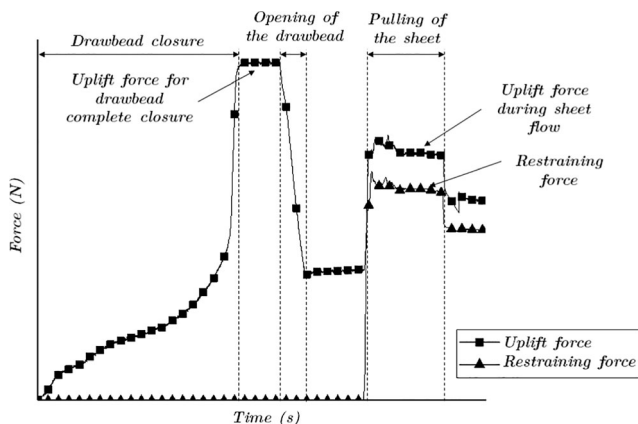

Fig. 8 Evolution of uplift and restraining forces during a drawbead restraining test

The sensitivity analysis covers three different major aspects that play an important role in the definition of the model: the mechanical properties of the sheet material, the contact between the sheet and tool and the geometry of the tools. Table 5 presents the parameters evaluated and their respective defined values.

For each parameter, a baseline value representing the real behaviour during the experimental tests, and a variation for this value, was defined. A brief explanation of the criteria considered in defining the variations follows. In terms of material properties, six different parameters were evaluated. The real Young modulus of the material measured in the tensile tests carried out is 198 GPa. Various previous works, such as Pavlina et al. [33], proved that the elastic modulus decreases with accumulated plastic strain. Xue et al. [34] observed a reduction of up to 24% of elastic modulus for the material DP780 with an accumulated plastic strain of 6%. The deformations at the drawbead are higher than this accumulated plastic strain, and a reduction of 24% for the elastic modulus was suggested in the present work. The variation value proposed for the elastic modulus was thus 150 GPa. The second material parameter that was analysed is the yield strength of the material. The supplying standard tolerance applied for the yield strength is 10% of the baseline value, or 540 MPa for the DP780 material analysed in the present work. The variation value proposed thus amounted to 594 MPa (in this case, the true stress-true strain curve was shifted up without modifying the material's hardening behaviour). With regard to the isotropic hardening of the material, the hardening law was modified by changing the α value in the Combined Swift-Hockett Sherby model. The baseline value of α was 0.25, which usually fits the behaviour of such materials as DP780 well. The variation value defined in the present work for α value was 1,
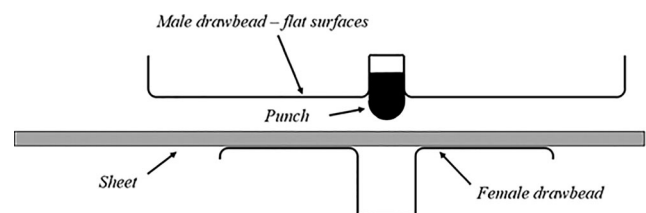

Fig. 9 Depiction of the parts involved in the simulation

Table 4 Parameters used to define the isotropic hardening of the material using the Swift-Hockett Sherby model

Material	Q (MPa)	σ_i (MPa)	σ_{sat} (MPa)	a	p	α	ε_0	m
DP780	1174	551	1071	12.5	0.853	0.250	0.001	0.072

indicating that the material was saturated rapidly and therefore showed lower values of hardening.

Concerning the kinematic hardening of the material, previous work, such as that of Lee et al. [28], showed the effect of this material property on the restraining forces. The work revealed differences of up to 25% in the restraining force when moving from an isotropic behaviour to a kinematic behaviour. However, no previous work evaluated the impact of the material's kinematic behaviour on the uplift force. For this purpose, a Chaboche kinematic hardening model was implemented in the model. The parameters of the Chaboche kinematic model were taken from [35], who conducted a tension-compression test on DP780 steel and identified parameters that better fit the behaviour of the material. The parameters are given in Table 6.

With regard to anisotropy, DP780 is a moderately low anisotropic material. In order to evaluate the impact of this phenomenon, values of DX54D (see Table 1) were thus artificially introduced into the DP780 material model. In this way, the difference between both cases was studied. Finally, variation in the thickness of the sheet was also evaluated. Industry references were considered yet again, and a variation of 4% in thickness was proposed. Consequently, the baseline value for the thickness amounted to 1.49 mm, while the variated value in the thickness was 1.55 mm. In terms of tribological behaviour, the uplift force using the real coefficient of friction presented in Fig. 2 and frictionless behaviour was compared.

The last aspect that was analysed was the geometrical definition of the drawbead. Commonly, an ideal perfect geometry is used in the numerical model definition. In reality, however, geometrical errors may exist that can affect the drawbead's response. The main purpose of the analysis in terms of geometrical definition was to evaluate the impact of such geometrical errors on the uplift force predicted by the numerical model. As a result, seven different variations were proposed in the geometrical definition of the drawbead. The first four variables refer to the dimensions of the drawbead. A variation of 10% for the inlet/outlet radius, the punch radius and the punch height was proposed. As for the female width, a variation of 0.5 mm was proposed. Another aspect that was taken into account encompasses potential deviations in the different surfaces making up the drawbead. During the machining and final polishing of the areas adjacent to the drawbead, geometrical errors may occur; as a result, the surfaces adjacent to the drawbead punch may not be completely parallel to one another. Furthermore, elastic deformations of the tools during the drawbead closure phase can also have an impact on the final geometry of the surfaces. In order to analyse this effect, three different misalignments were generated, as represented in Fig. 10.

Dashed lines in Fig. 10 represent the geometry of the misalignments proposed. The deviation of point O′ for the three misalignments is 0.1 mm, and only one of the sides of the drawbead was misaligned. It must also be mentioned that the

Table 5 Parameters and their values considered during the sensitivity analysis

Parameter under consideration		Defined values Baseline/variation
Material parameter	Young modulus (GPa)	198/150
	Yield strength (MPa)	540/594
	Isotropic hardening	Normal/low
	Kinematic hardening	No/yes
	Yield criteria	Isotropic/anisotropic
	Thickness (mm)	1.49/1.55
Contact parameter	Coefficient of friction	μ(contact pressure)/0
Geometric parameter	Female width (mm)	14.5/14.0
	Inlet/outlet radius (mm)	3/3.3
	Punch radius (mm)	5/5.5
	Punch height (mm)	3/3.3
	Dimensional variation I	No/asymmetric closure type I
	Dimensional variation II	No/asymmetric closure type I
	Dimensional variation III	No/parallel deviation

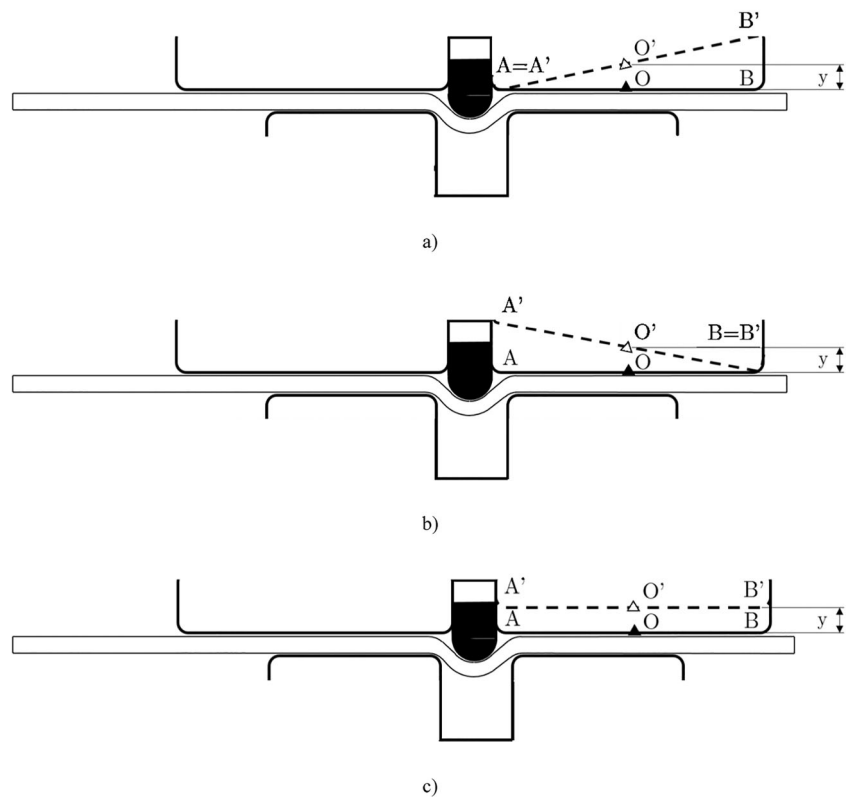**Table 6** Parameters that Sun and Wagoner found for the material DP780

σ_0	C_1	C_2	γ	Q	B
454	17062	517	72	163	16

geometrical misalignment has been overscaled in the graphic representation in order to give the reader a better understanding of the proposed deviations. The angle between the theoretical surface and the tilted surface was 0.2° for both asymmetric closure type I and asymmetric closure type II. In the case of the parallel deviation misalignment, the distance remained constant and amounted to 0.1 mm.

4 Results and discussion

Tables 7 and 8 show the experimental results obtained using the experimental drawbead tester developed in this work. Not all the different punch heights have been used for each material. DX54D and DP780 have been considered representative materials for mild steels and high-strength steels and all the drawbead punch heights have been analysed. In parallel, since HSLA180 is a drawing steel, punch heights of 4 mm and 5 mm have been analysed. For the rest of the materials, and because they are high-strength and ultra-high-strength steels,

Table 7 Experimental uplift force results

Material	Uplift force (N/mm)			
	Punch height (mm)			
	2	3	4	5
DX54D	25.7 ± 1.8	33.6 ± 3.1	42.1 ± 4.3	52.0 ± 4.2
HSLA180	-----	-----	61.7 ± 2.7	74.2 ±1.6
ZStE380	184.5 ± 11.7	222.3 ± 9.1	367.7 ± 4.1	-----
DP600	339.1 ±11.6	359.5 ± 16.3	594.9 ± 16.9	-----
DP780	447.0 ± 38.3	586.6 ± 62.1	709.8 ± 50.9	831.0 ± 21.3
Fortiform1050	581.3 ± 12.8	800.0 ± 38.8	961.5 ± 88.6	-----

punch heights of 2 mm, 3 mm and 4 mm have been analysed. Although the research work focuses on the comprehension of the drawbead closure and the uplift force generated, restraining forces are given as complementary information for the readers.

The obtained results are in agreement with what was expected. As the height of the punch increases, both the restraining and the uplift force increase. Moreover, the higher the resistance or thickness of the material is, the greater the uplift and restraining forces are. When comparing the uplift and the restraining forces, it can be observed that higher punch

Fig. 10 Graphic representation using dashed lines of the geometrical deviations generated in the drawbeads. Asymmetric closure type I (a), asymmetric closure type II (b) and parallel deviation (c)

Table 8 Experimental restraining force results

Material	Restraining force (N/mm)			
	Punch height (mm)			
	2	3	4	5
DX54D	31.2 ± 0.9	36.2 ± 0.4	43.2 ± 0.5	50.2 ± 1.4
HSLA180	-----	-----	59.2 ± 1.4	65.6 ± 0.7
ZStE380	161.2 ± 3.7	197.6 ± 3.6	240.8 ± 4.4	-----
DP600	243.4 ± 5.1	308.7 ± 4.9	371.9 ± 5.3	-----
DP780	258.9 ± 7.0	390.5 ± 8.8	-----	-----
Fortiform1050	387.9 ± 9.5	-----	-----	-----

Fig. 11 Evolution of the closing force for the different punch heights of the DP780

heights require very similar uplift and restraining forces. However, when the height of the punch is reduced, the ratio between the uplift force and the restraining force increases, so more force is necessary to close the drawbead than the restraining force that the drawbead applies to the sheet. When analysing each of the punch heights separately, it can be observed that when the strength of the material increases, the ratio between the uplift force and the restraining force decreases. For example, the ratio between the uplift and restraining forces in the case of DX54D steel and a punch height of 2 mm is 1.21. The ratio in the case of the Fortiform1050 for the same punch height is 0.66.

Another aspect that can be observed in the experimental results is the higher standard deviation observed in the uplift force when compared to the restraining force. Five tests have been carried out for each of the configurations and types of test. In the case of the uplift force, the average standard deviation when considering all the different punch heights and materials is 5.71%. On the other hand, the average standard deviation for the restraining force when considering all the different punch heights and materials is 1.98%. No trend has been observed concerning the standard deviation when analysing the different punch heights or material strengths. However, it can be concluded that it is more difficult to achieve a high level of repeatability in the uplift force experimental tests. The main reason for this lower level of repeatability is the sharp change in the uplift force that occurs during the complete closure of the drawbead.

Furthermore, the capacity of the numerical model explained in the previous section to determine the uplift force has been evaluated. Figure 11 shows the comparison between the numerical and experimental results of the DP780 with the different punch height conditions that have been studied. It can be appreciated that the numerical results predict at a high level of accuracy the evolution of the force along the closing of the drawbead. Only relevant differences are found at the final closure of the drawbead. As mentioned in Section 1, this was already observed by Kim et al. [17], who showed that the
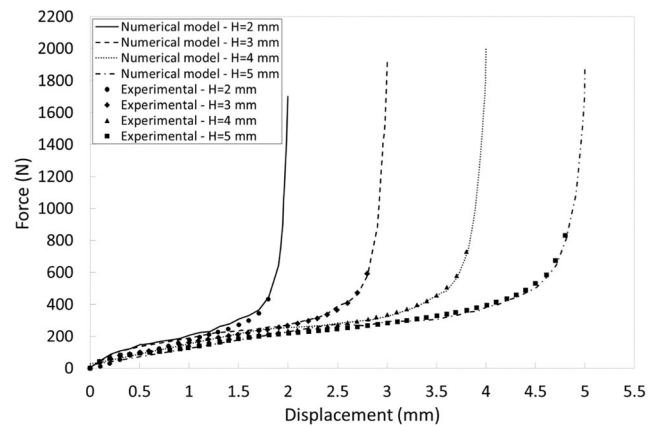
numerical results deviate from the experimental results in the last hundredths of a millimetre before the complete closure of the tools. Nevertheless, the accuracy of the developed numerical model has been validated, as it is able to reliably reproduce the closing force evolution in positive agreement with the experimental results. Another aspect that must be highlighted, and that was also mentioned by Kim et al., is that the numerical predicted uplift forces are much higher than the experimental measured uplift forces.

Because the numerical predictions for a perfect closing are much higher than the experimental results, a sensitivity analysis has been carried out to understand the reason for these differences. Figure 12 shows the results of the sensitivity analysis (variables defined in Table 5) where the effect of the selected parameters on the uplift force is quantified.

It can be observed that in terms of material properties, yield strength and material thickness have the greatest effect on the uplift force. The force increment is almost lineal with respect to the yield strength and more pronounced in the case of the thickness (a thickness increment of 4% results in a force increment of 16%). With regard to the friction modelization, almost no differences have been observed when changing the friction parameter from frictionless to pressure-dependent friction. Even though the bibliographic references pointed out that this parameter is very important in terms of restraining force, no influence has been found with respect to the uplift force (in agreement with Triantafyllidis et al. [27]). Finally, from the point of view of the geometry of the drawbead, the misalignments generated in the flat surfaces that lie in the lateral area of the punch have the greatest impact on the uplift force. Although the misalignment has been generated in only one of the sides, an uplift force reduction of up to 22% has been observed in two of the cases. This large reduction is observed in both cases where the misalignment is in the area close to the punch (asymmetric closure type II and parallel deviation misalignment). On the other hand, no significant force reduction has been observed when the

Fig. 12 Uplift force maximum value variation with respect to the base value for each parameter
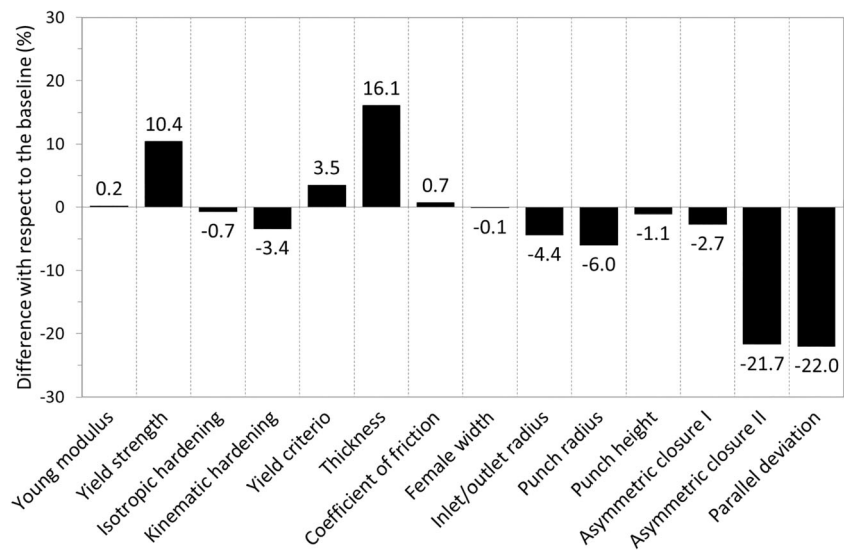

misalignment is far from the drawbead punch (asymmetric closure type I).

It can therefore be concluded that minimum deviations from an ideal geometry can result in significant differences in the uplift force results. In this regard, it can be stated that the differences between the numerical predictions and the experimental measurements lie in the lack of assurance of perfect contact between the surfaces during the final closure of the tool. This is a key factor to consider when attempting to predict industrial forces because, due to the tool elastic deformations that are produced during closing and the geometrical deviations that the tool may have after its machining and hand polishing, an important difference between numerical and experimental results can be found in terms of uplift force. It must also be taken into consideration that in order to achieve an homogeneous contact between the tool surfaces and to counteract the elastic deformation, the different components of industrial stamping tools are generally manually spotted during their initial try-out phase [8]. This way the geometrical deviations between the different contact surfaces are very much reduced which in fact can give as a result an evolution of the uplift forces during the try-out phase. For this reason, and as pointed out in Section 5, the development of analytical models able to predict the evolution of force over the drawbead closure becomes crucial.

The conclusions of the sensitivity analysis show that the flat surfaces on the lateral side of the punch have an important effect on the final uplift force when closing the drawbead. Taking advantage of the numerical model, a new analysis has been carried out. The model has been run using baseline values for all parameters and the force evolution along the closing of the tools has been measured. The force evolution is represented in Fig. 13. As observed, at the beginning of the closure, the force is localized on the punch surface. However, at the end of the closure, the force increment is produced on

the flat surfaces, dominating the total uplift force. In this case, the force produced in these surfaces is 86.5% of the total uplift force, which agrees well with the results obtained by Larsson et al. [25]. Moreover, in agreement with previous research [17], it can be observed that there is a relevant force increment in the last twenty hundredths of millimetres before complete closure, which uniquely affects the flat surfaces of the drawbead. This result is also in agreement with the observations made in the sensitivity analysis, where the flat surfaces on the lateral side of the punch were misaligned by 0.1 mm.

With the importance of the flat surface alignment in mind and assuming the difficulty of experimentally reproducing a perfect closure of the drawbead, an analysis for identifying the closing distance at which the numerical predictions match the experimental results has been carried out. In this case, in addition to the DP780 steel that was used in the sensitivity analyses, DX54D steel has also been considered in order to cover a wider range of mechanical properties and material thicknesses. Figure 14 shows the results for DX54D mild steel
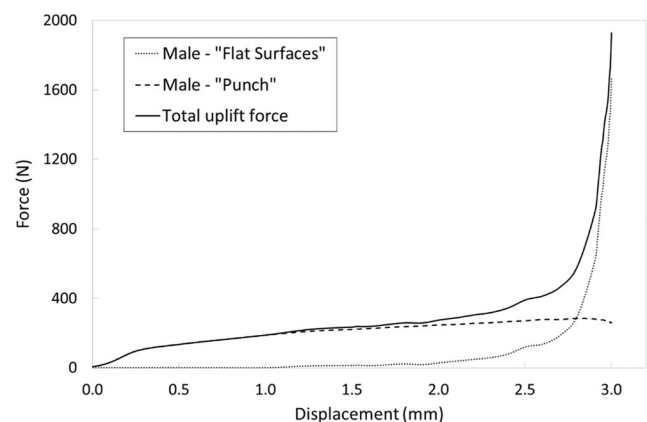
Fig. 13 Evolution of the forces generated in the tools along the drawbead closing (punch height of 3 mm and material DP780)
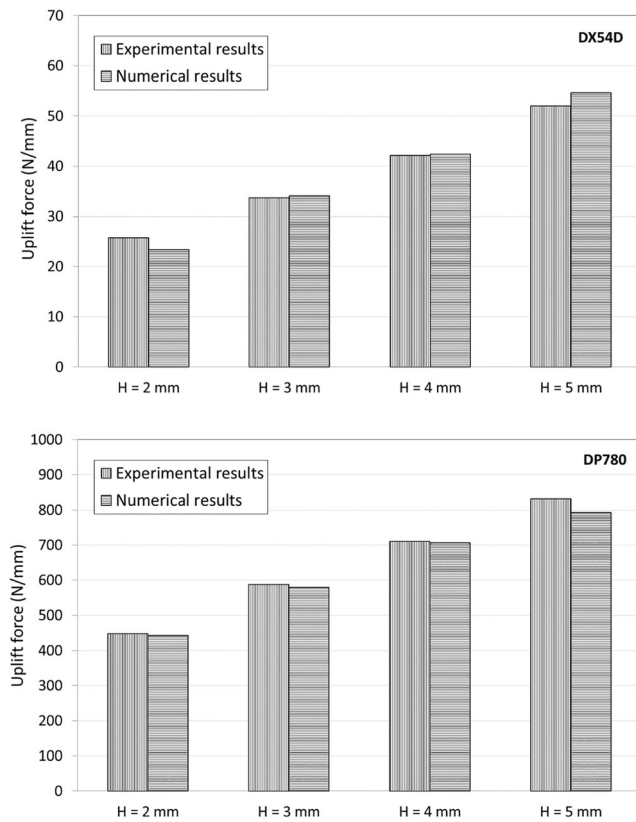
Fig. 14 Comparison of numerical and experimental uplift forces (numerical force at 0.2 mm from the perfect closing)

and for DP780 high-strength steel. The numerical closing distance at which the numerical and experimental force difference is at a minimum is 0.2 mm for both materials. The average error for DX54D material is 5.2% with a maximum error of 9.8% at a drawbead height of 5 mm. In the case of the DP780 material, the average error is 1.7% with a maximum error of 4.3% for a drawbead height of 5 mm.

5 Conclusions

The present work has analysed the force required to close the drawbead and has found that almost 90% of the required force is generated at the flat surfaces on the lateral side of the punch. The results substantially agree with previous research that determined that the uplift force was mainly governed by these surfaces.

The importance of the geometrical definition of these flat surfaces in the uplift forces has also been analysed, demonstrating that a misalignment of 0.1 mm in one side results in a force reduction of up to 22%. For this reason, it is also concluded that the lack of flat surfaces in experimental setups, such as the one proposed by Nine [4], or the measurement of the uplift force at a certain distance to a perfect closure,

such as in the experiments carried out by previous authors mentioned on the state of the art review, is the main reason for the underestimation of the uplift forces occurring in previous studies. Concerning the mechanical modelization of the material, it was found that the yield stress of the material is the most influencing material parameter in the uplift force. And finally, concerning the tribological modelization, it was found that the coefficient of friction does not have an impact in the calculation of the uplift force.

Considering previous conclusions, a new drawbead tester has been developed with the appropriate configuration including the flat surfaces on the lateral side of the drawbead punch. Furthermore, the measurement of the uplift force has been carried out without leaving any distance to perfect closure. Six different materials have been evaluated under different drawbead configurations and a database of uplift and restraining forces has been generated. The goal of the authors is to provide the academic community with reliable experimental data to be used as a database in order to improve current analytical models or develop new analytical models to be used as equivalent drawbead models.

The impact of the flat surfaces on the uplift force and the difficulty of generating perfect geometrical surfaces in real experimental setups together explain the differences between the experimental and numerical results obtained in the research work. The authors have found that the numerical predictions of the uplift force at 0.2mm of the perfect closure match well with the obtained experimental results. Differences for the materials analysed are lower than 5%.

The final conclusion is that, considering the real industrial non-ideal conditions, new analytical models, in contrast to current analytical solutions, should be able to predict the evolution of the uplift force over the drawbead closure. This way, after an initial learning phase, each user should be able to determine at which distance to perfect closure the analytical model accurately predicts the uplift force for his/her application. This solution is more flexible and allows the analytical model to fit the necessities of different users with different working procedures. The research group is already working on this solution and the development of a semi-analytical uplift force prediction model is currently underway.

Declarations

References

1. Alves JL, Bouvier S, Oliveira MC, Menezes LF (2005) Drawbeads: To be or not to be. In: AIP Conference Proceedings. AIP, pp 655–660

2. Courvoisier L, Martiny M, Ferron G (2003) Analytical modelling of drawbeads in sheet metal forming. J Mater Process Technol 133:359–370. https://doi.org/10.1016/S0924-0136(02)01124-X

3. Li SP, Güner A, Tekkaya AE (2015) Analysis of drawbead behaviour for sandwich sheets in sheet forming simulation. Appl Mech Mater 794:59–66. https://doi.org/10.4028/www.scientific.net/AMM.794.59

4. Nine HD (1978) Drawbead forces in sheet metal forming. In: Mechanics of Sheet Metal Forming. Springer US, Boston, pp 179–211

5. Nine HD (1982) The applicability of Coulomb's friction law to drawbeads in sheet metal forming. J Appl Metalwork 2:200–210. https://doi.org/10.1007/BF02834038

6. Bolay C, Essig P, Kaminsky C, Hol J, Naegele P, Schmidt R (2019) Friction modelling in sheet metal forming simulations for aluminium body parts at Daimler AG. IOP Conf Ser Mater Sci Eng 651:012104. https://doi.org/10.1088/1757-899X/651/1/012104

7. Gil I, Mendiguren J, Galdos L, Mugarra E, Saenz de Argandoña E (2016) Influence of the pressure dependent coefficient of friction on deep drawing springback predictions. Tribol Int 103:266–273. https://doi.org/10.1016/j.triboint.2016.07.004

8. Leocata S, Senner T, Saubiez J-M, Brosius A (2019) Influence of binder pressure zones on the robustness of restraining forces in sheet metal forming. Procedia Manuf 29:209–216. https://doi.org/10.1016/j.promfg.2019.02.128

9. Triantafyllidis N, Maker B, Samanta SK (1986) An analysis of drawbeads in sheet metal forming: part I—problem formulation. J Eng Mater Technol 108:321–327. https://doi.org/10.1115/1.3225889

10. Maker B, Samanta SK, Grab G, Triantafyllidis N (1987) An analysis of drawbeads in sheet metal forming: part II—experimental verification. J Eng Mater Technol 109:164–170. https://doi.org/10.1115/1.3225957

11. Stoughton TB (1988) Model of drawbead forces in sheet metal forming. In: Proceedings of the 15th biennial IDDRG Congress. Dearborn,pp 205–215

12. Sanchez LR, Weinmann KJ (1996) An analytical and experimental study of the flow of sheet metal between circular drawbeads. J Eng Ind 118:45–54. https://doi.org/10.1115/1.2803647

13. Wang N-M (1982) A mathematical model of drawbead forces in sheet metal forming. J Appl Metalwork 2:193–199. https://doi.org/10.1007/BF02834037

14. Keum YT, Kim JH, Ghoo BY (2001) Expert drawbead models for ® nite element analysis of sheet metal forming processes. Int J Solids Struct 38:5335–5353

15. Kim Y, Choi W (1993) A study of the method of evaluation of the frictional characteristics of Zn·Ni coated steel sheets. J Mater Process Technol 36:187–197. https://doi.org/10.1016/0924-0136(93)90030-A

16. Yang YY, Jin ZH, Wang RF, Wang YZ (2002) 2D elasto-plastic FE simulation of the drawbead drawing process. J Mater Process Technol 120:17–20. https://doi.org/10.1016/S0924-0136(01)01052-4

17. Kim C, Im Y, Heo Y et al (1997) Finite-element analysis and experimental verification for drawbead drawing processes. J Mater Process Technol72:188–194. https://doi.org/10.1016/S0924-0136(97)00149-0

18. Firat M (2008) An analysis of sheet drawing characteristics with drawbead elements. Comput Mater Sci 41:266–274. https://doi.org/10.1016/j.commatsci.2007.04.014

19. Green DE (2005) Description of Numisheet 2005 Benchmark #3 Stage-1: channel draw with 75% drawbead penetration. In: AIP Conference Proceedings. AIP, pp 894–904

20. Moon SJ, Lee MG, Lee SH, Keum YT (2010) Equivalent drawbead models for sheet forming simulation. Met Mater Int 16:595–603. https://doi.org/10.1007/s12540-010-0812-2

21. Barlat F, Brem JC, Yoon JW, Chung K, Dick RE, Lege DJ, Pourboghrat F, Choi SH, Chu E (2003) Plane stress yield function for aluminum alloy sheets—part 1: theory. Int J Plast 19:1297–1319. https://doi.org/10.1016/S0749-6419(02)00019-0

22. Chaboche JL (1986) Time-independent constitutive theories for cyclic plasticity. Int J Plast 2:149–188. https://doi.org/10.1016/0749-6419(86)90010-0

23. Xu SG, Bohn ML, Weinmann KJ (1997) Drawbeads in sheet metal stamping - a review. SAE Technical Paper 970986, 1997. https://doi.org/10.4271/970986

24. Choi TH, Huh H, Chun BK, Lee JH (1997) Draw-bead simulation by an elasto-plastic finite element method with directional reduced integration. J Mater Process Technol 63:666–671. https://doi.org/10.1016/S0924-0136(96)02704-5

25. Larsson M (2009) Computational characterization of drawbeads. J Mater Process Technol 209:376–386. https://doi.org/10.1016/j.jmatprotec.2008.02.009

26. Yellup JM, Painter MJ (1985) The prediction of strip shape and restraining force for shallow drawbead systems. J Appl Metalwork 4:30–38. https://doi.org/10.1007/BF02833674

27. Triantafyllidis N, Maker B, Samanta SK (1986) An Analysis of drawbeads in sheet metal forming : part I — problem formulation. J Eng MaterTechnol 108:321–327. https://doi.org/10.1115/1.3225889

28. Lee MG, Chung K, Wagoner RH, Keum YT (2008) A numerical method for rapid estimation of drawbead restraining force based on non-linear, anisotropic constitutive equations. Int J Solids Struct 45:3375–3391. https://doi.org/10.1016/j.ijsolstr.2008.02.008

29. Sriram S (2006) Contact pressure distribution for flow of metal through drawbeads. https://doi.org/10.4271/2006-01-0787

30. Sigvant M, Pilthammar J, Hol J, Wiebenga JH, Chezan T, Carleer B, den Boogaard T (2019) Friction in sheet metal forming: influence of surface roughness and strain rate on sheet metal forming simulation results. Procedia Manuf 29:512–519. https://doi.org/10.1016/j.promfg.2019.02.169

31. Li KP, Carden WP, Wagoner RH (2002) Simulation of springback. Int J Mech Sci 44:103–122. https://doi.org/10.1016/S0020-7403(01)00083-2

32. Agirre J, Galdos L, Saenz de Argandoña E, Mendiguren J (2018) Hardening prediction of diverse materials using the digital image correlation technique. Mech Mater 124:71–79. https://doi.org/10.1016/j.mechmat.2018.05.007

33. Pavlina EJ, Lin C, Mendiguren J, Rolfe BF, Weiss M (2015) Effects of microstructure on the variation of the unloading behavior of DP780 Steels. J Mater Eng Perform 24:3737–3745. https://doi.org/10.1007/s11665-015-1671-2

34. Xue X, Liao J, Vincze G, Pereira AB, Barlat F (2016) Experimental assessment of nonlinear elastic behaviour of dual-phase steels and application to springback prediction. Int J Mech Sci 117:1–15. https://doi.org/10.1016/j.ijmecsci.2016.08.003

35. Sun L, Wagoner RH (2013) Proportional and non-proportional hardening behavior of dual-phase steels. Int J Plast 45:174–187. https://doi.org/10.1016/j.ijplas.2013.01.018